Electron transport studies in rhombohedral series of Al-doped $LaMnO_{3+\delta}$: an effective medium approach

2000 J. Phys.: Condens. Matter 12 7887

(http://iopscience.iop.org/0953-8984/12/36/304)

J. Phys.: Condens. Matter **12** (2000) 7887–7903. Printed in the UK PII: S0953-8984(00)13392-2

Electron transport studies in rhombohedral series of Al-doped $LaMnO_{3+\delta}$: an effective medium approach

R V Krishnan and A Banerjee

Inter University Consortium for DAE Facilities, University Campus, Khandwa Road, Indore 452 017, India

Received 10 April 2000, in final form 31 July 2000

Abstract. We report the electron transport studies in the rhombohedral $LaMn_{1-x}Al_xO_{3+\delta}$ series ($0 \leqslant x \leqslant 20\%$) of samples. Though all the samples are ferromagnetic below a transition temperature (T_C), only the samples with $x \leqslant 5\%$ exhibit a metal–insulator transition (MIT) at T_C while the samples with $x \geqslant 10\%$ are all semiconducting above and below T_C. The sample with $x = 7.5\%$ is a borderline case where MIT at T_C is immediately taken over by semiconducting behaviour at lower temperatures. Thus a progressive crossover from ferromagnetic–metallic state to ferromagnetic–insulating state is observed in this series within the same structure. This is accompanied by a decrease in Mn^{4+} content across the magnetic and conduction percolation thresholds. This systematic crossover from a double exchange dominated regime to an exclusively superexchange regime, preserving the rhombohedral symmetry, makes the present series an important and unique one for the study of electron transport in the colossal magnetoresistance manganites. An effective medium approach is employed to explain the resistivity behaviour in this series over the whole temperature range, which gives strong support for polaronic conduction in all the samples. This polaronic conduction justifies the presence of dynamic Jahn–Teller effects in the samples and the change in the character of polarons across T_C illustrates the role of electron–lattice interaction as well as its coupling to magnetic states (core spins) of the samples. The dominance of double exchange is evident from metallic resistivity in the samples with $x \leqslant 5\%$ which have Mn^{4+} much above the percolation threshold for metallicity. However the observed non-trivial temperature dependence of metallic resistivity could not be explained by double exchange alone and it is shown in this study that one needs to take into account superexchange interactions even in the double exchange dominated regime to understand the electron transport, thus supporting the current understanding in these pervoskite manganites.

1. Introduction

Mixed valence perovksite manganites have enjoyed a recent resurgence owing to the interest they have created in fundamental issues like colossal magnetoresistance (CMR), orbital and charge ordering and spontaneous phase segregation besides their potential place in technological applications such as solid oxide fuel cells, magnetoresistive sensors etc. The profound influence of defect chemistry and the crystal structure on the physical properties of these mixed valence compounds is exemplified in the rich magnetic and electronic phase diagrams [1–3]. The comparable values of different interaction energies like the bandwidth (W), charge-transfer energy (Δ_{CT}), on-site Coulomb energy (U_{dd}), exchange energy (J) and crystal field energies in the manganites leads to a strong interplay of charge, spin and lattice degrees of freedom [4].

One of the key issues that has been investigated intensely in the hole-doped lanthanum manganites is the occurrence of the metal–insulator transition (MIT) [5]. It is generally

0953-8984/00/367887+17$30.00

observed that the MIT occurs around the ferromagnetic transition temperatures and the observed CMR is the greatest only around the MIT peak temperatures, thus pointing to an important connection between magnetism and electrical conductivity. This connection was first qualitatively explained by Zener via the double exchange (DE) mechanism [6]. Later modifications of the DE model due to DeGennes and Anderson *et al* explained MIT as a natural consequence of increase in hopping probability of the itinerant e_g electrons amidst a matrix of ferromagnetically aligned core (t_{2g}) spins [7]. An important requirement of the DE mechanism is the random distribution of mixed valent Mn ions (Mn^{4+} and Mn^{3+}), which can be produced either by non-stoichiometry or by divalent-ion (hole) doping in the La site of the parent $LaMnO_3$. MIT occurs around 14% of Mn^{4+} content, which marks the percolation threshold for metallic conduction and persists up to ∼35% of Mn^{4+} content beyond which the ordering of Mn^{3+} and Mn^{4+} ions inhibits the e_g electron hopping [5]. Besides these defect chemistry requirements, it is also found that lattice effects and other local structural modifications profoundly affect the charge transport in the manganites. For example, the orthorhombic and rhombohedral distortions reduce the Mn–O–Mn bond angle from 180° of the ideal cubic structure, which, in turn, reduces the orbital overlap. Consequently there is a great variation in transport properties of these three structures. This can be inferred from the fact that MIT is observed only in rhombohedral and cubic structures although all the three structures can have ferromagnetism. Further evidences for the coupling between charge transport and lattice are rightly exemplified in many other experimental observations as well [5].

The need to understand the innate relationship between electron transport and magnetic ordering along with lattice effects is also equally felt in the recent past. Although the DE model could explain the metallic state coexisting with the ferromagnetic ordering, it did not take into account the lattice effects and other local structural modifications. Furthermore, the qualitative temperature dependence of resistivity in the ferromagnetic–metallic state as predicted from the DE model is found to be discrepant with the experimental observations and the absolute value of resistivity calculated from the DE model was a few orders of magnitude smaller than the experimental value. These observations led Millis *et al* to propose that DE alone is not sufficient to explain the experimental data and that strong electron–lattice coupling has to be taken into account [8]. In particular, dynamic Jahn–Teller (JT) effects are conceived to be a strong source of electron–lattice coupling and this prediction has already been affirmed by recent experiments [9]. On the other hand, the observation of CMR in certain pyrochlore manganites with no DE interactions has indicated that DE is not a necessary ingredient for the exotic physical properties exhibited by manganites in general [10]. Of late, the importance of ferromagnetic superexchange Mn^{3+}–O–Mn^{3+} interactions in the presence of dynamic JT effects has increasingly been realized, thus pointing out the inadequacy of DE interactions in the ferromagnetic metallic regime in these CMR manganites [11]. Despite the plethora of studies in this direction, the understanding of the interrelationship between charge transport, magnetism and lattice effects is far from complete. Many open problems still exist, which include the nature of metallic state, the relative importance of double exchange and superexchange interactions and the role of lattice effects in charge transport in these perovskite manganites. In this complex scenario, the problem of understanding the electron transport properties in CMR manganites is addressed well by

(i) choosing a crystal structure that is more relevant to CMR compositions;

(ii) choosing a series of samples with the same crystal structure where the changes in lattice parameters are minimal with no other complications (ionic size mismatch, magnetic dopant etc) across the whole series;

(iii) choosing a series of samples where there is a continuous variation of DE strength across both the magnetic and conduction percolation thresholds so that the relative importance of DE and SE interactions can be explicated more effectively. This would then facilitate a systematic understanding of the interplay of DE and SE interactions in the ferromagnetic metallic state and plausibly in the paramagnetic insulating state as well.

With this motivation, we have carried out a thorough study of magnetic and transport properties in a series of samples where Al is substituted in the Mn site of the rhombohedral phase of lanthanum manganite. All the samples of the series, $LaMn_{1-x}Al_xO_{3+\delta}$ with $0 \leqslant x \leqslant 20\%$, crystallize in rhombohedral ($R\bar{3}c$) symmetry with only marginal changes in lattice parameters. With increase in Al content, it is found that Mn^{4+} content varies continuously from ~25% to 0%, thus marking a progressive transition from the DE dominated regime to an exclusively SE regime across the series. In a recent communication, we have explained this transition of DE to SE ferromagnetism across the series and we give here the essential results of our magnetic study [11]. All the samples exhibit a transition from paramagnetic to ferromagnetic state with a well defined T_C and T_C is found to decrease systematically with increase in Al content. Lower doped samples ($x \leqslant 5\%$) are found to have dominant DE ferromagnetism owing to the preponderance of Mn^{4+} content. The ferromagnetism of the intermediate compositions ($x = 7.5$ and 10%) is found to be governed sensitively by a stiff interplay of both DE and SE ferromagnetism while the higher Al doped samples ($x \geqslant 15\%$) are governed by exclusively SE ferromagnetic Mn^{3+}–Mn^{3+} interactions assisted by dynamic Jahn–Teller effects. The present communication is a sequel of our earlier paper and we focus here on the electron transport properties of the Al-doped $LaMnO_{3+\delta}$.

Dc and low frequency resistivity measurements have been carried out on the series of samples in the temperature range 77–300 K. All the samples of the series $LaMn_{1-x}Al_xO_{3+\delta}$ show activated behaviour in the paramagnetic regime ($T > T_C$). Samples with $x \leqslant 5\%$ show insulator–metal transitions around respective ferromagnetic transitions (T_C) indicated by the change in sign of $(d\rho/dT)$ at T_C. Although there are a few humplike features just below T_C, all these samples remain metallic at the lowest temperatures. The residual resistivity in the metallic regime of all these samples is a few orders of magnitude higher than the maximum metallic resistivity (Mott's criterion: $\rho_{Mott} \sim 5$–10 mΩ cm) expected for metallic oxides. Further, the temperature dependence of resistivity in the metallic regime is quite deviated from the simple linear form expected for a typical metal. The sample with $x = 7.5\%$ also shows a MIT at T_C. However just below T_C there occurs a steep upturn in resistivity, making the sample semiconducting again at lower temperatures. All the samples with $x \geqslant 10\%$ are semiconducting with progressively increasing negative temperature coefficient of resistivity. We have quantitatively analysed the temperature dependence of resistivity both in the paramagnetic and ferromagnetic regimes by means of a mean field model, namely the effective medium approximation, which treats the observed resistivity as an effective balance of resistivity contributions from the SE and DE bonds, distributed randomly in the samples. Polaronic hopping conduction seems to be the most probable mechanism governing the electron transport in all the samples. Activation energies for all these samples below T_C are consistently lower than the values above T_C indicating the profound influence of magnetic ordering on resistivity. Although double exchange assisted metallic conduction plays the dominant role for samples with $x \leqslant 5\%$, giving metallicity for these samples below T_C, semiconducting contributions of superexchange interactions must also be considered to explain successfully some of the features in the metallic regime of these samples. To the best of our knowledge, such a detailed analysis of electron transport in both the ferromagnetic and paramagnetic regimes by effective medium approach in rhombohedral series of samples as carried out in the present work is the first of its kind.

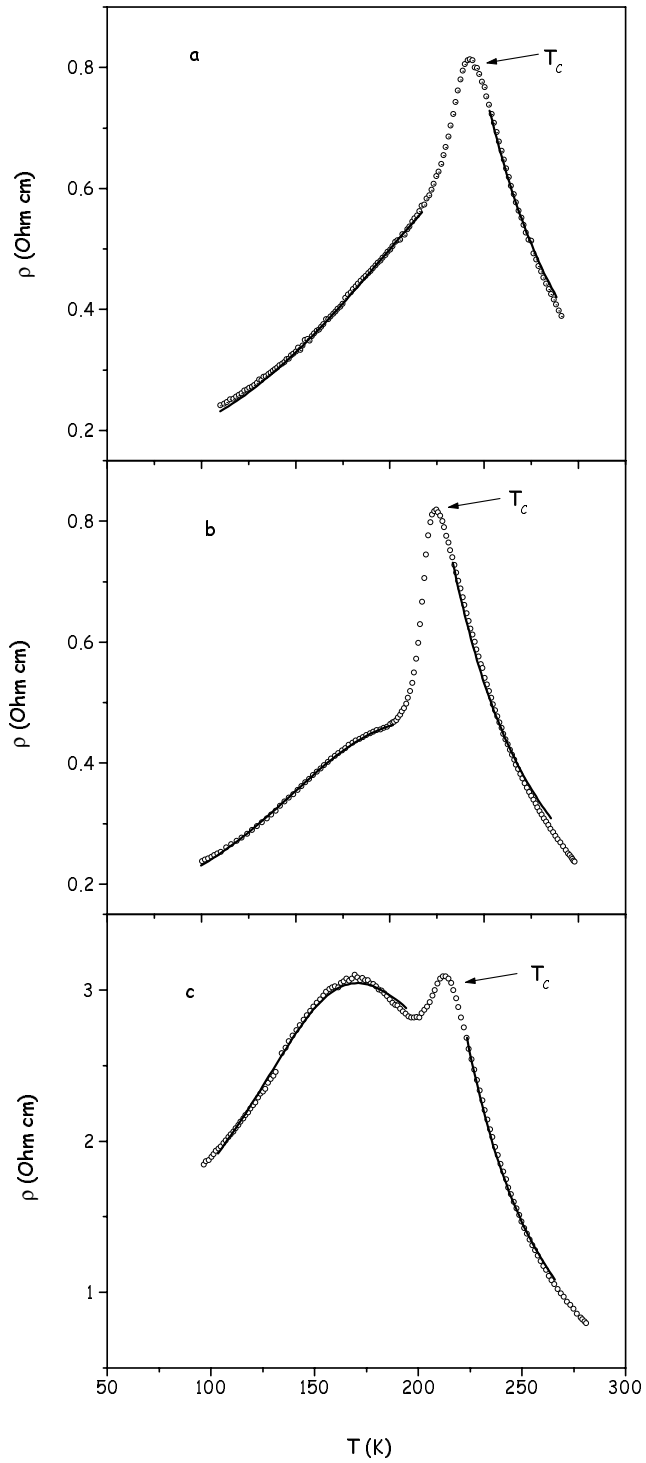

Figure 1. Temperature dependence of resistivity for (a) $x = 0$, (b) $x = 2.5$ and (c) $x = 5\%$ samples. Solid lines are the EMA fits to equation (1) in the paramagnetic regime ($T > T_C$) and the ferromagnetic regime ($T < T_C$).

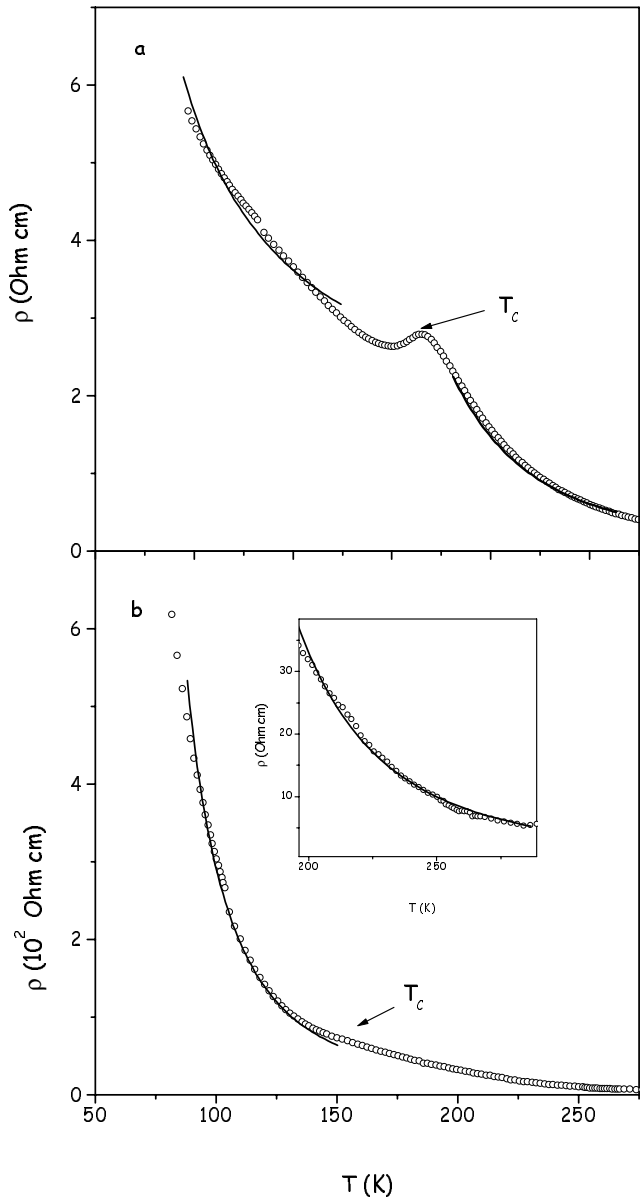

Figure 2. (a) Temperature dependence of resistivity for the $x = 7.5$ sample (symbols). Solid lines are the EMA fits to equation (1) in the paramagnetic regime ($T > T_C$) and the ferromagnetic regime ($T < T_C$). (b) Temperature dependence of resistivity (symbols) and EMA fit to equation (1) (solid line) for the $x = 10\%$ sample in the ferromagnetic regime. The inset shows the same in the paramagnetic regime.

2. Experimental details

Polycrystalline samples of the series $La\,Mn_{1-x}Al_xO_{3+\delta}$ with $0 \leqslant x \leqslant 20\%$ have been prepared by a standard solid state ceramic route with ($\geqslant$99.9% pure) starting materials La_2O_3, MnO_2 and Al_2O_3. All the samples are found to crystallize in rhombohedral symmetry with only

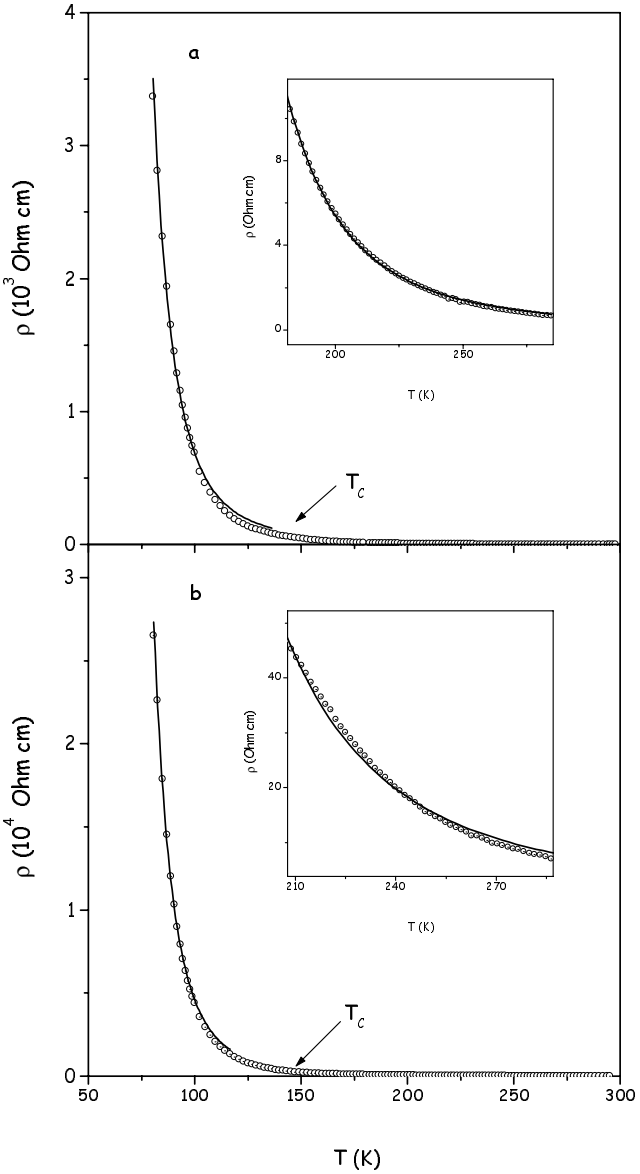

Figure 3. Temperature dependence of resistivity for (a) $x = 15$ and (b) $x = 20\%$ samples. Solid lines are the EMA fits to equation (1) in the ferromagnetic regime ($T < T_C$). Insets of both (a) and (b) show the observed resistivity (symbols) and EMA fit (solid line) in the paramagnetic regime for $x = 15$ and 20% samples respectively.

marginal changes in structure and lattice parameters. The detailed synthesis procedure and structural characterization details are given in [11]. Relevant parameters are given in table 1. Dc resistance and low frequency (up to 133.33 Hz) ac resistance measurements were made in the standard four-probe geometry. We observed that the ac and dc resistivity data match very well, indicating that the measured resistivity is intrinsic to all the samples. Some of the compositions in this series were also prepared by the nitrate route and these samples had

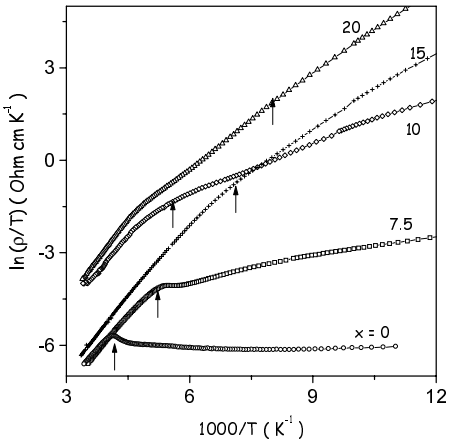

Figure 4. Representative small polaron conduction plots in the entire temperature range for the series $LaMn_{1-x}Al_xO_{3+\delta}$. Arrows indicate the respective T_C for the samples at which there is a discernable change in slope of the curves.

almost the same peak values of resistivity and other qualitative features as found for the samples prepared by ceramic route. Figures 1–3 show the temperature dependence of resistivity in all the samples prepared by the ceramic route.

3. Analysis of the results

3.1. Effective medium approach

As seen in figures 1–3, the nature of resistivity changes around the ferromagnetic transition temperature (T_C) for samples with $x \leqslant 5\%$ thus marking a MIT as magnetic ordering sets in. There is a MIT even for $x = 7.5\%$ at T_C but the semiconducting nature is stabilized at lower temperatures. Although there is no MIT for samples with $x \leqslant 10\%$ there is indeed a characteristic change of slope at T_C (figure 4). These features point to a strong relationship between magnetic phases and resistivity behaviours in our samples particularly below the magnetic ordering temperature. Thus any quantitative analysis of resistivity below T_C must necessarily take into account this connection. All the samples of the series remain ferromagnetic, despite the gradual crossover from double exchange dominance to exclusively superexchange interactions. It is therefore expected that the progressive transition from ferromagnetic metallic state to ferromagnetic insulating state observed in the present series is due to this interplay of superexchange and double exchange interactions. With this basis we attempt to understand the resistivity results by analysing the combined influence of these magnetic exchange interactions on electron transport in our samples. The observed resistivity at any temperature is understood as the effective resistivity of a 3D matrix where the SE and DE bonds are randomly distributed, and the temperature dependence of the resistivity follows naturally from the particular forms assumed for these individual bonds. We have thus analysed our resistivity data throughout the measured temperature range by means of a mean field model, namely the effective medium approximation. This treats the SE and DE contributions to resistivity in a bond percolation framework. We shall now explain briefly the conceptual premise of this treatment.

The effective medium approximation (EMA) was originally conceived for understanding electrical conduction in composite materials [12]. The classical limits of this theory were later invoked for the study of electronic conduction in disordered materials where hopping among localized states well below the mobility edge was the main interest [13]. The basic premise of this approximation is that the material under consideration is assumed to be a homogeneous, random mixture of two types of bond with different conductances and the conduction in the composite is essentially studied as a percolation problem. The conduction in such a bond percolation scenario is indeed decided by the 'strength' of these two individual bonds as well as the ratio of these two bond fractions. For a typical three-dimensional case the effective conductivity of the composite is given by the following expression [12]:

$$\rho = \frac{4\rho_1\rho_2}{\{(3p-1)\rho_1 + (2-3p)\rho_2\} + [\{(3p-1)\rho_1 + (2-3p)\rho_2\}^2 + 8\rho_1\rho_2]^{1/2}} \tag{1}$$

where ρ_1 and ρ_2 are the resistivity contributions of the two types of bond. The percolating variable p, is identified with the volume fraction of those bonds for which the resistivity is ρ_2. For instance, if we assume that ρ_1 and ρ_2 are respectively the nonmetallic and metallic bond contributions in a random mixture of such bonds, the EMA model predicts a transition between metallic and nonmetallic states across a percolation threshold, p_c, of the metallic bonds. This value depends sensitively on the dimensionality of the system and for metallic conduction in a 3D matrix, $p_c = 1/3$. Around this value the effective resistivity ρ is a crucial function of the ratio (ρ_1/ρ_2). On the other hand, if both ρ_1 and ρ_2 are nonmetallic contributions with different functional forms, then the effective resistivity will be predominantly decided by only one of these on either side of the percolation threshold value. Investigations on the continuous random resistor networks by Kirkpatrick *et al* and others have proved the success of this EMA model in different contexts [12, 14]. Recently a similar approach had been adopted by Rao *et al* to explain magnetoresistance properties in one of the CMR compositions [15]. In the following section we validate the applicability of the effective medium approximation in our samples to analyse the electrical conduction.

3.2. EMA analysis of the series $LaMn_{1-x}Al_xO_{3+\delta}$

In the ensuing analysis of resistivity in terms of the EMA model, we have fitted the temperature dependence of measured resistivity to equation (1), where we have assumed ρ_1 and ρ_2 to represent the resistivity of the superexchange bonds (Mn^{3+}–O–Mn^{3+} and Mn^{4+}–O–Mn^{4+}) and double exchange bonds (Mn^{3+}–O–Mn^{4+}) respectively. The percolating variable p is identified with the volume fraction of DE bonds. This analysis has been carried out in both paramagnetic and ferromagnetic regimes independently.

From table 1 we note that there is a gradual reduction in Mn^{4+} from ∼25% to ∼0%, with a corresponding depletion of DE bonds across the series. Thus one has a situation where one goes from a dominance of DE interactions where the volume fraction of DE is far above the percolation threshold for metallic conduction ($x \leqslant 5\%$) to a state where there are no DE bonds at all ($x \geqslant 15\%$) and this gives rise to a progressive transition from metallic to insulating phase across the series. We can thus model our samples in the ferromagnetic regime as homogeneous, random mixtures of SE and DE bonds. It is important to note that the fractions of these individual bonds differ for each sample in the series. Since these bonds are randomly distributed in all the samples, the effective resistivity will not be a simple series or a parallel combination of these two contributions and one has to resort to a mean field treatment of all the bonds such as the effective medium approximation. This validates the applicability of the EMA model to the present series. Also the statistical distribution of SE and DE bonds is the same in both the paramagnetic and ferromagnetic regimes since the amount and distribution

of Mn^{3+} and Mn^{4+} ions do not change with temperature for a given sample. EMA analysis can therefore be carried out both below and above T_C equivalently, the only difference being that there is a qualitative change in temperature dependence of DE bonds at T_C and there are changes in the parameters of the SE resistivity contribution as well. As we shall see in the later discussion, such an analysis on either side of the magnetic transition is an important handle to probe the effect of magnetic ordering on electron transport.

In the paramagnetic regime both DE and SE bonds are assumed to have a thermally activated semiconduction form, whereas in the ferromagnetic regime only SE bond has a semiconduction form and DE bond is assumed to be a metallic bond. These assumptions are in consensus with Zener's original idea of metallic conduction owing to ferromagnetic ordering in the DE model [6]. Besides it is also generally observed that double exchange ferromagnets are metallic conductors in the magnetically ordered state while semiconduction is the hallmark of superexchange systems.

It remains now to choose physically viable forms to describe the temperature dependence of ρ_1 and ρ_2. At the first sight it would seem appropriate to choose a simple linear-T dependent form for the DE bond ($\rho \propto T$) and a simple thermally activated conduction form for the SE bond ($\rho \propto \exp(1/T)$). As one can see from figure 1, the samples which are metallic at low temperatures ($x \leqslant 5\%$) do not exhibit a simple linear temperature dependence of resistivity that is expected from a simple metal. Attempts had been made in a few earlier studies to explain such a nontrivial metallic resistivity by including the effects of electron–electron interactions, electron–magnon interactions and the effects of disorder etc [2, 3]. We adopt particularly the form assumed in the work of Schiffer *et al* where the authors had fitted the metallic regime resistivity to the forms $\rho_{DE} \propto T^{2.5}$, which the authors had interpreted as an empirical fit accounting for the above mentioned interactions [3]. Regarding the semiconduction form of resistivity, it was found that neither a simple thermal activation nor the variable range hopping (VRH) conduction forms fit well our observed data in the entire temperature range. On the other hand the small polaron hopping conduction was found to fit more accurately the measured resistivity for all the samples in the paramagnetic regime and for samples with $x \geqslant 7.5\%$ in the ferromagnetic regime. It is therefore assumed in the present analysis that SE resistivity is governed by small polaron hopping: $\rho_{SE} \propto [T \exp(1/T)]$. This particular choice has an advantage that it incorporates naturally the electron–lattice interactions which stem from dynamic Jahn–Teller (JT) effects in our samples. Further this assumption is in consensus with the current scenario in electron transport in manganites [16, 17].

It is worthy to mention a few points regarding the succeding analysis. First of all, we have considered every sample to be a simple homogeneous, random mixture of SE and DE bonds of definite strength assumed to be unaffected by granularity and disorder effects. Grain boundary effects seem to be negligible in our samples as inferred from the perfect agreement between dc resistivity and low frequency ac resistivity measurements. This ensures that the measured resistivity is intrinsic to the samples. Second, we have neglected the effects of the nonmagnetic bonds due to Al in the present analysis. This is justifiable because the maximum amount of nonmagnetic Al doping in our series is only 20% (far below the percolation threshold for the loss of ferromagnetism). Finally, we have considered the percolation in a sort of averaged microscopic network of bonds and translated the whole analysis to bulk behaviour. No attempt is made to systematically evolve this bond percolation problem into cluster percolation problem and then to bulk resistivity to explain the critical regime ($T \rightarrow T_C$) and thus EMA analysis has been carried out for temperature range not very close to T_C. As we shall see below, even this simple-minded application of the EMA model to our series renders physically meaningful results.

We have fitted the resistivity data for all the samples to equation (1) with the following parameters.

- *Paramagnetic regime*:

$$\rho_{SE} = \rho_0 T \exp(E_0/k_B T)$$
$$\rho_{DE} = \rho_0' T \exp(E_0'/k_B T). \tag{2}$$

- *Ferromagnetic regime*:

$$\rho_{SE} = \rho_1 T \exp(E_1/k_B T)$$
$$\rho_{DE} = \rho_1' + \rho_2 T^{2.5}. \tag{3}$$

The fitted curves are shown by thick solid lines in figures 1–3 and the fitting parameters are given in table 2.

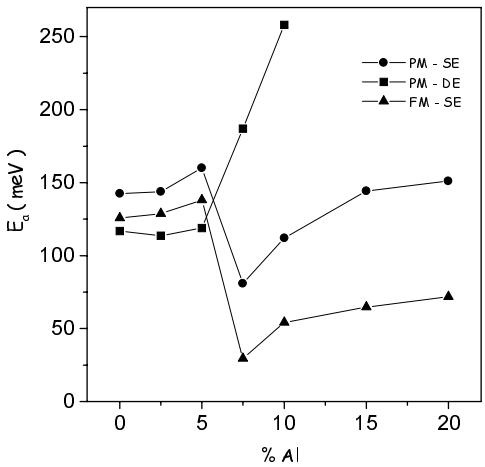

Figure 5. Variation of SE and DE activation energies obtained from EMA analysis in the paramagnetic (PM) and ferromagnetic (FM) regimes.

4. Discussion

In perovskite manganites, oxidation of MnO_6 octahedra by the introduction of divalent cations and/or cation vacancies, particularly Mn vacancies, is expected to perturb the periodic potential seen by the e_g electrons and with the reduction in temperature these mobile holes tend to become trapped at Mn sites adjacent to divalent cations or vacancies that introduced them [18]. In the classic paper of DeGennes, the same idea had been discussed in terms of self-trapped carriers [7]. Since all the samples in the present series belong to the same rhombohedral structure, where dynamic JT distortions are known to be dominant, considerable electron–lattice coupling is feasible, thus favouring polaron formation in our samples due to incomplete delocalization of electrons. Evidence of these dynamic JT effects had already been found to stabilize ferromagnetism in our samples [11]. The progressive decrease in Mn^{4+} content (reduction in mobile holes) with simultaneous increase in Al^{3+} content (increasing Mn site disorder) might therefore facilitate electron localization more vehemently. This justifies the feasibility of polaronic conduction in the present series of samples. From our preliminary thermopower measurements on the $x = 0\%$ sample of our series, we found the activation energy in the paramagnetic regime to be around 20 meV while the activation energy for the same sample from resistivity measurements yielded ∼140 meV in the same temperature range. Mott had described this large difference in the two activation energies to be a strong indication of polaronic conduction [19].

4.1. Paramagnetic regime

As the samples are cooled from room temperature towards the ferromagnetic transition temperature (T_C) the transport behaviour in all the samples is found to be activated. Analysing the SE and DE contributions with the small-polaron hopping form as mentioned above, the EMA analysis gives two values of activation energies E_0 and E_0' corresponding to the SE and DE contributions respectively in equation (2). The variation of these values with Al content in the paramagnetic regime is shown in figure 5. For $x \leqslant 5\%$, we note that E_0 remains always higher than E_0' and there is a sharp fall in E_0 for $x = 7.5\%$. For $x \geqslant 10\%$ this value increases with increase in Al content. On the other hand E_0' remains almost constant for the samples with $x \leqslant 5\%$. At $x = 7.5\%$ there is a sharp rise in E_0' and for $x \geqslant 7.5\%$, E_0 always exceeds E_0'. This trend of activation energies can be understood as follows. A lower value of activation energy for a bond implies a lesser resistance for that bond. The above variation of E_0 and E_0' with Al doping therefore implies that for samples with $x \leqslant 5\%$, DE conduction is more favourable than the SE conduction whereas the opposite is true for the samples with $x \geqslant 10\%$. The cross-over between these two trends occurs at $x = 7.5\%$, thus marking a transition from dominance of DE interactions to that of SE interactions. This sharp fall is almost identical with the variation of Mn^{4+} content across the series. From table 1 we observe that Mn^{4+} content remains almost the same ($\sim$25%) for $x \leqslant 5\%$ and at $x = 7.5\%$ the Mn^{4+} content falls sharply to 14%, which is around the percolation threshold for DE metallic conduction. Since DE and SE strengths depend on (Mn^{3+}–Mn^{4+}) and (Mn^{3+}–Mn^{3+}) interactions respectively, a great reduction in Mn^{4+} content at $x = 7.5\%$ is accompanied by a corresponding reduction in DE strength too. This explains the sharp fall in E_0 and the sharp rise in E_0' for this sample. For the sample with $x = 10\%$ SE interactions dominate because of the much reduced Mn^{4+} ($\sim$7%) and for $x \geqslant 15\%$ there are only SE interactions.

Overall, the activation energy values obtained in our samples compare well with the values reported in earlier studies [20, 21]. Owing to Jahn–Teller distortions prevalent in our samples, a predominant contribution to activation energy is expected to come from lattice effects though other contributions of magnetic and coulombic origin may also be present. The maximum variation of activation energy across the series is only $\sim$20%. This indicates that the Jahn–Teller polarons are responsible for these observed values since there is no large change in structural and lattice parameters across the series. Otherwise the changes in activation energies would have been much larger. Dionne had earlier proposed that electrons become self-trapped at the Curie temperature, with an activation energy nearly equal to the exchange energy [22]. Obviously this is not true in our case where activation energies are much higher than the exchange energy ($\sim k_B T_C$) for all the samples, thus substantiating a large nonmagnetic contribution to activation energy.

The prefactors ρ_0 and ρ_0' are inversely related to the polaron diffusion constant D as it can be shown by the following expression for the small-polaron resistivity [17, 19]:

$$(\rho/T) = \frac{k_B}{n(1-x)e^2 D} \exp(E_a/k_B T) = \rho_0 \exp(E_a/k_B T) \tag{4}$$

where n is the charge carrier density ($\sim 10^{20}$ cm^{-3}), x is the hole (Mn^{4+}) content and D is the polaron diffusion constant. The polaron diffusion constant for a typical cubic coordination can be given explicitly as $D = \frac{1}{6} a^2 \nu$ where a is the lattice constant and ν is the attempt frequency ($\sim 10^{14}$ s^{-1}) which corresponds to the optical phonon frequency [19, 23]. We see from table 2 that there is only a small variation in both ρ_0 and ρ_0' across the series, implying that the polaron diffusion constant D has remained almost the same both in the SE and DE contributions with Al-doping. However for a given sample ρ_0' is always lower than ρ_0. This is probably due to a larger vacant density of states at the Mn^{4+} sites and hence due to a larger rate of hopping

between heterovalent Mn ions than between homovalent Mn ions. We calculated the polaron diffusion constants (D) for our samples using the values of ρ_0 and ρ_0' from table 2 and from equation (4). The calculated values of D lie in the range of 10^{-2}–10^{-4} cm^2 s^{-1} and the attempt frequencies calculated from these D values ($\sim 10^{12}$–10^{14} Hz) are in good agreement with those found in earlier works [19, 23].

4.2. Ferromagnetic regime

Transition from the paramagnetic to ferromagnetic state has a profound influence on the electron transport in all the samples of the series. The essential results of the EMA analysis in the ferromagnetic regime are summarized below:

- First of all, there is a qualitative change in DE contribution at T_C where the semiconduction form goes over to metallic form. This leads to the observed metal–insulator transition at T_C in the DE dominated regime ($x \leqslant 5\%$).
- Although there is no change in functional form for SE contributions below T_C there is a marked change in the parameters of the ρ_{SE} form below T_C in all the samples. For example, the activation energy (E_0) is considerably reduced for the whole series of samples in the ferromagnetic regime.
- Even in the DE dominated regime ($x \leqslant 5\%$), the observed features in resistivity could not be explained by only the DE form. For instance, the assumed metallic temperature dependence alone cannot explain the lower temperature resistivity hump for $x = 2.5$ and the resistivity peak for $x = 5\%$ samples. This can be fitted only with some competing interactions taken into account. In the present case it is the SE contribution with the opposite temperature dependence besides the metallic form of DE contribution. Thus an effective medium treatment becomes a necessary rather than a sufficient condition for the analysis of resistivity in these samples. As we can see from figure 1, EMA treatment reproduces these features very well.
- The increasing dominance of SE interactions over the DE interactions for $x \geqslant 7.5\%$ is also tracked well by the EMA analysis (figures 2 and 3), where it is found that the effective resistivity corresponds more to $\rho_{SE}(T)$.
- In the DE contribution, ρ_1' is found to change only a little with increase in Al content as compared with the coefficient of the temperature-dependent term (ρ_2) which increases monotonically across the series.

Now we shall try to understand the influence of the ferromagnetic transition on the EMA fitting parameters.

There is growing evidence in the manganite literature for an observable crossover at T_C from large-polaron hopping ($T < T_C$) to small polaron hopping ($T > T_C$). Small polarons are typified by large effective mass, smaller radius and hence larger activation energy [24]. The observed decrease in activation energy E_0 below T_C can be understood as due to such a change in polaronic character induced by ferromagnetic ordering. It was originally postulated by Mott that at low temperatures ($T < \Theta_D$), a polaron in a crystal moves with a well defined wavevector $\boldsymbol{k}$ and an effective mass m_p given by

$$m_p = \frac{\eta}{2m_e\omega R^2} \exp\left(\frac{2W_H}{\eta\omega}\right) \tag{5}$$

where m_e is the free electron mass, R is the hopping distance (typically 4 Å for transition metal oxides), W_H is the activation energy involved in polaron hopping and ω is the optical phonon frequency mentioned earlier [19]. By using equation (5) and from the values of activation

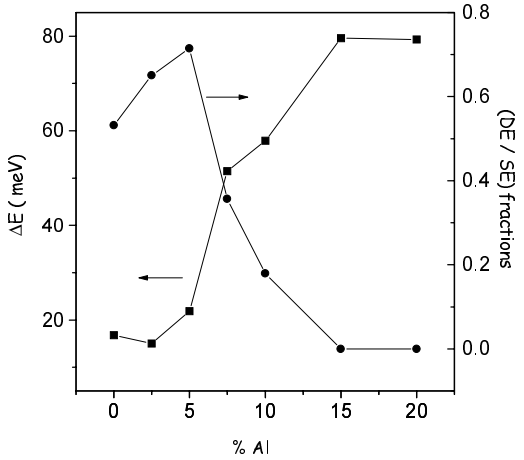

Figure 6. Difference in activation energy $\Delta E = E_0 - E_1$ and the ratio of DE to SE fractions calculated from table 1, plotted as a function of Al content.

energies taken from table 2, we had calculated the mass enhancement in all our samples. In the paramagnetic regime m_p was roughly 7 m_e in all the samples whereas it was found to be around 5 m_e in the ferromagnetic regime, thus supporting the picture of small-polaron to large-polaron crossover across the ferromagnetic transition. Interestingly similar value had been obtained by Jaime *et al* from their high-temperature thermopower measurements on manganite samples [23]. Alternatively by assuming an $m_p = 6\,m_e$ (typically one MnO_6 octahedron), the calculated hopping distance turns out to be of the order of 5–6 Å. This corresponds to the value of lattice constant in our samples and justifies further our assumption of small-polaron conduction in the present series of samples [24]. Also we note from figure 5 that the difference between the SE activation energies of the paramagnetic and ferromagnetic regimes is not constant for all the samples. The difference is hardly 20 meV for the samples with $x \leqslant 5\%$ whereas it is appreciably large (∼80 meV) for the samples with $x \geqslant 10\%$. This stems from the variation in SE and DE strengths across the series. In figure 6, we plot this difference in activation energy ($\Delta E = E_0 - E_1$) as a function of Al doping. Also shown in the figure is the ratio of DE to SE fractions (table 1). It is readily seen that the activation energy difference has an inverse correlation with the ratio of DE to SE fractions (strengths). This further supports the observed crossover between DE and SE interactions as one goes beyond $x = 10\%$ in the ferromagnetic regime. We have observed such a crossover in our magnetic measurements also, thus proving that the changes in the magnetism in the present series are reflected in electron transport properties too [11].

We observe that ferromagnetic ordering has not changed the values of ρ_1 in the SE contribution as compared with the values in the paramagnetic regime. This is understandable because the polaron diffusion constant is not expected to change much in the absence of any large changes in crystal structure or lattice parameters in the whole series as one goes across T_C. The attempt frequency ν calculated according to equation (4) in the whole series of samples was of the order of 10^{13}–10^{15} Hz in accordance with the observations of earlier workers [19, 23].

In the DE contribution to resistivity, it is found that ρ_1' changes only marginally across the series. This factor is expected to give information about the temperature independent contributions to resistivity such as grain boundary effects, domain wall scattering, defects and cation vacancies. It may be concluded from table 2 that these effects are roughly the same with

Table 1. Percentage contents of Al^{3+}, Mn^{3+} and Mn^{4+} and fraction of DE and SE bonds in the series $LaMn_{1-x}Al_xO_{3+\delta}$.

%Al (x)	%Mn^{4+}(y)	%Mn^{3+}($1-x-y$)	Fraction of DE bonds $2y(1-x-y)$	Fraction of SE bonds $y^2+(1-x-y)^2$
0	21	79	0.332	0.668
2.5	24	73.5	0.353	0.598
5	25	70	0.350	0.553
7.5	14	78.5	0.220	0.636
10	7.4	82.6	0.122	0.688
15	0	85	0	0.723
20	0	80	0	0.640

Table 2. Effective medium approximation fitting parameters for the series $LaMn_{1-x}Al_xO_{3+\delta}$.

	Paramagnetic regime			Ferromagnetic regime				
%Al	ρ_0 (Ω cm K^{-1})	E_0 (meV)	ρ_0' (Ω cm K^{-1})	E_0' (meV)	ρ_1 (Ω cm K^{-1})	E_1 (meV)	ρ_1' (Ω cm)	ρ_2 (Ω cm $K^{-2.5}$)
0	9.5×10^{-4}	142.5	2.9×10^{-7}	116.8	7.0×10^{-4}	125.7	3.1×10^{-3}	1.4×10^{-8}
2.5	8.0×10^{-4}	143.7	2.5×10^{-7}	113.7	1.1×10^{-4}	128.7	3.5×10^{-3}	1.7×10^{-8}
5	1.6×10^{-4}	160.0	7.2×10^{-7}	118.8	1.2×10^{-4}	138.1	2.6×10^{-2}	1.6×10^{-7}
7.5	0.8×10^{-4}	88.7	1.5×10^{-7}	185.0	1.3×10^{-3}	34.1	8.4×10^{-2}	3.0×10^{-5}
10	2.0×10^{-4}	112.0	3.5×10^{-7}	258.1	8.5×10^{-3}	54.1	8.5×10^{-2}	2.5×10^{-3}
15	6.0×10^{-6}	144.3	—	—	3.4×10^{-3}	64.7	—	—
20	5.0×10^{-5}	151.1	—	—	9.7×10^{-3}	71.8	—	—

increase in Al doping. However the effects of Al doping are strongly seen in the variation of the factor ρ_2 which is a measure of combined effects of electron–electron and electron–magnon interactions and we find this factor to be monotonically increasing with x. Relatively small values of ρ_2 for $x = 0$ and 2.5% samples show the predominance of DE interactions. In previous studies, this term had been found to be strongly field dependent, giving rise to the observed colossal magnetoresistance [2, 3]. It is worth noting in the present series that, for the samples where DE is dominant, the values of ρ_1' and ρ_2 are in excellent agreement with those obtained by Schiffer *et al* for similar DE ferromagnetic compositions [3].

The absolute value of resistivity in the metallic samples is at least a few orders of magnitude higher than the Mott criterion for maximum resistivity (5–10 mΩ cm) in metallic oxides [19]. This is usually attributed to the narrow 3d band of these oxides and strong effects of disorder in the metallic regime. This leads to the observed nonlinear temperature dependence and higher values of resistivity. This fact is exemplified well in recent photoemission experiments on manganite compounds in the metallic regime where it is observed that there is at least a few orders of magnitude reduction in coherent Drude weight from that expected for a metal [25].

Thus we could explain all the features in resistivity of the present series, in both the ferromagnetic and paramagnetic regimes, by an effective medium treatment of SE and DE bonds. We understand the progressive transition from the ferromagnetic metallic (FMM) state to the ferromagnetic insulating (FMI) state as a consequence of the overwhelming dominance of SE over the DE interactions within the same crystal structure. The importance of dynamic JT effects has been emphasized in the context of polaron formation in these samples. Recent x-ray absorption measurements have revealed that these dynamic effects are found to persist

even in the metallic samples [26]. This explains the need to take the SE interactions also to reproduce the observed resistivity peak in $x = 5\%$ in the metallic regime below T_C. In essence, the dynamic Jahn–Teller distortions provide the necessary electron–phonon coupling and compete with the DE interactions to decide the conductivity in rhombohedral Al-substituted Lanthanum manganites.

The fact that FMM samples are qualitatively different from FMI samples is not surprising as evidenced in a few earlier reports on local structure investigations [9]. The essence of these studies is the observation of an abrupt broadening of certain pair distribution peaks in neutron diffraction data only in samples exhibiting MIT and the absence of such a feature in insulating samples in the same series, although ferromagnetism is observed in both. Further the local JT distortions were found to be homogeneous above the MIT peak and inhomogeneous below the MIT peak. These results indicate that the local structure and hence the character of polarons will be entirely different in FMM and FMI samples. These facts support our finding that there is a large change in polaronic activation energies obtained for the FMM and FMI samples.

The sample with $x = 7.5\%$ is at the boundary between the DE and SE dominated regimes. Since the Mn^{4+} content in this sample is around the percolation threshold for metallic conduction, DE and SE interactions are expected to have a stiff competition in this sample particularly at lower temperatures. Indeed this is the reason the MIT observed at T_C for this sample is immediately wiped away by the dominant SE interactions, thereby reverting to semiconducting nature at lower temperatures. This is marked by the steep upturn in resistivity below T_C (figure 2(a)). A similar behaviour had been earlier observed in $La_{1-x}Sr_xMnO_3$ ($x = 0.125, 0.15$) samples which was interpreted by Yamada *et al* as due to the progressive transition: polaron liquid (PM regime) $\rightarrow$ Fermi liquid (dirty metal regime) $\rightarrow$ polaron lattice (low-temperature semiconducting regime) [27]. Since the $x = 7.5\%$ sample has almost the same Mn^{4+} content as was in their LaSrMnO sample, it is quite likely that a similar interpretation holds good for this sample too. This further supports the idea of polaronic conduction in our samples even in the ferromagnetic regime. Although similar resistivity peaks were observed in $x = 2.5$ and 5% samples also, the preponderance of Mn^{4+} in these samples makes them metallic at much lower temperatures.

Before we conclude this discussion we would like to mention that from resistivity measurements alone we are not able to resolve the individual contributions of magnetic correlations and Jahn–Teller effects to polaron formation. Detailed frequency dependence of ac conductivity measurements may throw more light on the polaron dynamics in these samples. Also the effects of disorder on electron transport have to be consistently taken into account since such effects are known to change the polaron conduction appreciably. Therefore in the preceding analysis no attempt has been taken to separate out the contributions from magnetic and JT polarons to the observed activation energies. However it is found that there are substantial ferromagnetic correlations even far above T_C in the paramagnetic regime particularly for the higher Al-doped samples (figure 4). These may arise due to the formation of magnetic polarons in these samples. The major ingredients for the magnetic polaron formation are lattice distortion (to localize the carriers) and short-range ferromagnetic correlations. In the present series of samples, we have some evidences of such ferromagnetic correlations even in the paramagnetic regime from our magnetic measurements. For example the dc magnetization in low fields in samples with $x \geqslant 10\%$ in the present series showed that the zero-field cooled (ZFC) and field cooled (FC) curves do not match even above T_C, thus affirming the above conjecture that there exist larger spin clusters close to T_C. These together with the dynamic JT distortions could favour the magnetic polaron formation in our samples. Indeed the existence of similar spin clusters has earlier been inferred from small-angle neutron scattering, muon spin relaxation and electron paramagnetic resonance measurements [28].

5. Conclusions

We have presented a detailed report on electron transport studies on the series of $LaMn_{1-x}Al_xO_{3+\delta}$ ($0 \leqslant x \leqslant 20\%$) samples, which has shown a progressive crossover from the double-exchange dominated regime (ferromagnetic–metallic) to the exclusively superexchange regime (ferromagnetic–insulating) with change in composition, preserving the rhombohedral symmetry throughout the series. Such a progressive crossover from double exchange to superexchange interactions within the same rhombohedral symmetry, devoid of any other structural and magnetic complications, makes the present series unique and important in the context of perovskite CMR manganites. An effective medium approach has been adopted to explain the transport behaviour in all the samples over the whole measured temperature range. It is found that polaronic conduction plays an important role in the overall transport properties, suggesting strong electron–lattice coupling in all the samples. This gives an additional proof for the already inferred dynamic Jahn–Teller effects in the present series of rhombohedral samples. Further the coupling between charge transport and magnetism is evidenced by the observation of a change in the polaronic character across the magnetic transition temperatures. It is shown that double exchange alone is not adequate to explain the resistivity even in the double-exchange dominated metallic regime and that superexchange interactions are also necessary to explain these properties. This substantiates the current wisdom that DE alone is not adequate to explain the metallicity, ferromagnetism and CMR in the perovskite manganites. The effective medium approach carried out in the present series has yielded physically meaningful parameters such as polaron diffusion constants and effective polaron mass—in compliance with the values obtained from other measurements in similar compounds. Further measurements are in progress in this series of compounds to gain more insight into the interplay of DE and SE interactions and the mechanism of CMR as well as to elucidate the physical constants unequivocally.

Acknowledgments

We are grateful to Dr B A Dasannacharya for his keen interest in the work and many useful discussions. RVK acknolwedges UGC, India for a fellowship.

References

[1] van Roosmalen J A M, Cordfunke E H P, Helmholdt R B and Zandbergen H W 1994 *J. Solid. State Chem.* **110** 100
[2] Urushibara A, Moritomo Y, Arima T, Asamitsu A, Kido G and Tokura Y 1995 *Phys. Rev.* B **51** 14 103
[3] Schiffer P, Ramirez A P, Bao W and Cheong S-W 1995 *Phys. Rev. Lett.* **75** 3336
[4] Pickett W E and Singh D J 1996 *Phys. Rev.* B **53** 1146
[5] Ramirez A P 1997 *J. Phys.: Condens. Matter* **9** 8171 and references therein
Coey J M D, Viret M and von Molnar S 1999 *Adv. Phys.* **48** 167 and references therein
[6] Zener C 1951 *Phys. Rev.* **82** 403
[7] DeGennes P G 1960 *Phys. Rev.* **118** 141
Anderson P W and Hasegawa H 1955 *Phys. Rev.* **100** 675
[8] Millis A J, Littlewood P B and Shraiman B I 1995 *Phys. Rev. Lett.* **74** 5144
Roder H, Zhang J and Bishop A R 1996 *Phys. Rev. Lett.* **76** 1356
Millis A J, Shraiman B I and Mueller R 1996 *Phys. Rev. Lett.* **77** 175
[9] Dai P, Zhang J, Mook H A, Liou S H, Dowben P A and Plummer E W 1996 *Phys. Rev.* B **54** R3694
Argyriou D N, Mitchell J F, Potter C D, Bader S D, Kleb R and Jorgensen J D 1997 *Phys. Rev.* B **55** R11 965
Tyson T A, Mustre de Leon J, Conradson S D, Bishop A R, Neumeier J J, Roder H and Zhang J 1996 *Phys. Rev.* B **53** 13 985
[10] Subramanian M A, Toby B H, Ramirez A P, Marshall W J, Sleight A W and Kwei G H 1996 *Science* **273** 81

Troyanchuk I O, Efimov D A, Samsonenko N V, Shapocalova E F and Szymezak H 1998 *J. Phys.: Condens. Matter* **10** 7957
[11] Krishnan R V and Banerjee A 2000 *J. Phys.: Condens. Matter* **12** 3835
[12] Landauer R 1952 *J. Appl. Phys.* **23** 779
Kirkpatrick S 1971 *Phys. Rev. Lett.* **27** 1722
Last B J and Thouless D J 1971 *Phys. Rev. Lett.* **27** 1719
[13] Eggarter T P and Cohen M H 1970 *Phys. Rev. Lett.* **25** 807
Ambegaokar V, Halperin B I and Langer J S 1971 *Phys. Rev.* B **4** 2612
[14] Frisch H L, Hammersley J M and Welsh D J A 1962 *Phys. Rev.* **126** 949
Shante V K S and Kirkpatrick S 1971 *Adv. Phys.* **20** 325
[15] Rao G H, Sun J R, Sun Y Z, Zhang Y L and Liang J K 1996 *J. Phys.: Condens. Matter* **8** 5393
[16] Li J Q, Uehara M, Tsuruta C, Matsui Y and Zhao Z X 1999 *Phys. Rev. Lett.* **82** 2386
[17] Snyder G J, Hiskes R, Dicarolis S, Beasley M R and Geballe T H 1996 *Phys. Rev.* B **53** 14 434
[18] Goodenough J B 1997 *J. Appl. Phys.* **81** 5330
[19] Mott N F and Davis E A 1979 *Electronic Processes in Non-crystalline Materials* (New York: Oxford) 2nd edn
[20] Kertesz M, Reiss I, Tannhauser D S, Langpape R and Rohr F J 1982 *J. Solid State Chem.* **42** 125
van Roosmalen J A M, Huijsmans J P P and Plomp L 1993 *Solid State Ion.* **66** 279
[21] Kusters R M, Singleton J, Keen D A, McGreevy R and Hayes W 1989 *Physica* B **155** 362
[22] Dionne G F 1996 *J. Appl. Phys.* **79** 5173
[23] Jaime M, Salamon M B, Rubinstein M, Treece R E, Horwitz J S and Chrisey D B 1996 *Phys. Rev.* B **54** 11 914
[24] Holstein T 1959 *Ann. Phys., NY* **8** 343
[25] Okimoto Y, Katsufuji T, Ishikawa T, Arima T and Tokura Y 1997 *Phys. Rev.* B **55** 4206
[26] Subias G, Garcia J, Proietti M G and Blasco J 1997 *Phys. Rev.* B **56** 8183
[27] Yamada Y, Hino O, Nohdo S, Kanao R, Inami T and Katano S 1996 *Phys. Rev. Lett.* **77** 904
[28] Oseroff S B, Torikachvilli M, Singley J, Ali S, Cheong S-W and Schultz S 1996 *Phys. Rev.* B **53** 6521
Heffner R H, Le L P, Hundley M F, Neumeier J J, Luke G M, Kojima K, Nachumi B, Uemura Y J, MacLaughlin D E and Cheong S-W 1996 *Phys. Rev. Lett.* **77** 1869